Coulomb-nuclear interference in the inelastic projectile excitation of ^{20}Ne by ^{40}Ca

Nguyen Van Sen, G. Ratel, R. Darves-Blanc, J. C. Gondrand, and F. Merchez
Institut des Sciences Nucléaires, IN2P3 and USMG, B. P. 257, 38044 Grenoble, France
(Received 22 July 1977)

Coulomb-nuclear interference effects were investigated in the inelastic scattering of ^{20}Ne by ^{40}Ca with excitation of the first 2^+ state in ^{20}Ne. Measurements were performed at 54 and 60.5 MeV for the elastic and inelastic angular distributions and from 36 to 95 MeV for the excitation functions. The elastic data were analyzed in terms of the optical model. The inelastic results were compared with distorted-wave Born-approximation and coupled channel calculations. The reorientation effect was investigated.

[NUCLEAR REACTIONS ^{40}Ca(^{20}Ne, ^{20}Ne); $E = 54, 60.5$ MeV measured $\sigma(\theta)$; $E = 36$–95 MeV, measured $\sigma(\theta, E)$, $\theta = 20, 28, 36, 44, 52°$; for g.s., first 2^+ in ^{20}Ne. Optical model and DWBA analysis. Coupled-channel calculations with reorientation effects. Natural target.]

I. INTRODUCTION

Coulomb-nuclear interference effects in the inelastic scattering of charged nuclei near the Coulomb barrier can be understood in terms of semiclassical pictures[1] by writing the transition amplitude as a coherent sum of a long-range Coulomb excitation amplitude[2] and a nuclear amplitude of opposite sign localized predominantly at the nuclear surface. Earlier data could be reproduced by using this description in semiclassical theories[3,4] and in the distorted-wave Born-approximation (DWBA). Recently a different approach based on a closed-form quantal formalism[5] was developed for investigating the physical nature and origin of the interference structures in inelastic and elastic cross sections.

Good fits using DWBA have been obtained, particularly in the inelastic scattering of ^{16}O and/or ^{18}O from the first 2^+ states of Ni, Mo, Sr, and Sn isotopes.[6-8] These fits were comparable in quality to those provided by coupled-channel (CC) formalism[9] although the deformation length deduced from the CC calculations are expected to be more reliable. However, it has been found[6,8] that the DWBA calculations failed to reproduce the inelastic projectile-excitation for ^{18}O: The theoretical angular distributions for the ^{18}O (2^+, 1.98 MeV) state had to be shifted forward to fit the experimental data. Such a shift could be performed[8] by coupled-channel calculations taking into account the $0^+ - 2^+$ coupling together with the reorientations effects[2] provided by the coupling between the magnetic substates of the 2^+ level. It has been suggested[4] that the inelastic heavy ion scattering could then be used as a valuable tool for measuring static quadrupole moments which are responsible for the reorientation effects. In fact, an unreasonable large quadrupole moment was needed to explain the observed shift for the scattering ^{18}O(2^+) + ^{58}Ni studied by Videbaek *et al.*[8]: The theoretical quadrupole moment had to be taken equal to 6 times the experimental value. Similar results were obtained by Frahn and Rehm[5] using the closed-form formalism. The use of a collective macroscopic model for ^{18}O could be questionable[8] and multistep processes including higher levels might be needed.[8,10]

In the present work, the Coulomb-nuclear interference effects were investigated in the inelastic scattering of ^{20}Ne from ^{40}Ca leading to the excitation of the 2^+ 1.63 MeV level of ^{20}Ne. The excited nucleus can fairly be described by a prolate collective rotational model.[11,12] Moreover, the electromagnetic transition probability $B(E2)$ which determines the Coulomb excitation amplitude has been well known from a great number of experiments[13] and the static quadrupole moment of the 2^+ state considered has been obtained[14,15] with accuracy from measurements involving a very large Coulomb reorientation effect. The ^{20}Ne projectile should then permit a relevant investigation of the nuclear reorientation effect in the inelastic scattering with excitation of its first 2^+ state.

Measurements were performed at 54 and 60.5 MeV for the elastic and inelastic scattering angular distributions, and from 36 to 95 MeV in steps of about 3 MeV for the excitation functions. The elastic data were analyzed in terms of the optical model using a four-parameter complex potential.

The inelastic experimental results were compared with DWBA and coupled channel calculations.

II. EXPERIMENTAL METHOD AND RESULTS

The experiments were performed inside an 1m diam scattering chamber with ^{20}Ne beams furnished by the Grenoble isochronous cyclotron. Self-supporting natural Ca targets 100 μg/cm^2 thick were used. The energy spectra were obtained by means of surface barrier Si detectors. Three or five detectors were mounted at 6° or 8° lab. intervals on an arm movable around the target. In the opposite side of the incident beam direction were placed a monitor detector at a forward angle and a ΔE-E counter telescope whose spectra were two-dimensionally displayed so as to survey possible contributions of reaction products to the elastic and inelastic peaks of interest. Silicon detectors with thicknesses of 100–350 μm were used except for the telescope ΔE which was 14 μm thick. The aperture of each detector was limited by means of tantalum slits to an angular acceptance of about 0.5° and a solid angle of about 0.15 msr. The angular uncertainty on the detection angle was about ±0.05°. By means of a collimator the focused beam spot at the target position was limited to about 3 mm in diameter. Beam intensities from a few nA to 500 nA were collected during the experiments by a Faraday cup placed downstream the scattering chamber. The spectra of the multichannel analyzer were recorded for each measurement on magnetic tapes by a connected PDP-9 computer which was also used for off-line data reductions.

Angular distributions were measured at 54 and 60.5 MeV for the elastic scattering and the inelastic scattering leading to the excitation of the first 2$^+$ 1.63 MeV level of ^{20}Ne. Five excitation functions at 20°, 28°, 36°, 44°, and 52° lab were measured from 36 to 95 MeV in steps of about 3 MeV by using ^{20}Ne beams at 51.5, 55, 60, 69.7, 80 and 94.9 MeV and a rotating set of aluminum absorbers placed upstream before the target. The position of the elastic scattering peak on the monitor spectra was used for the relative energy calibration with an accuracy of about ±0.2%. The absolute energy of the incident beam were obtained with an uncertainty of about ±300 keV by measuring the magnetic stiffness with an analyzing magnet. In fact, the 60 and 80 MeV beams were used as absolute references, the other energies were deduced from the monitor relative calibration. The absorbers permitted to save beam operating time but deteriorated the beam energy resolution, so that the experimental results were only considered whenever the uncertainty due to the peak separation is less than 15%. The overall energy resolution was about 250–700 keV. In several cases, a peak-fitting routine was run for the peak separation. Reliable results for the inelastic scattering could be obtained whenever the excitation probability $d\sigma_{inel}/d\sigma_{el}$ is greater than about 0.01. Only fragmentary results could be deduced for the 3$^-$ 3.73 MeV level of ^{40}Ca whose excitation is one order of magnitude weaker than for the ^{20}Ne (2$^+$) as shown in Fig. 1. The excitation of the ^{20}Ne(4$^+$, 4.25 MeV) was not clearly observed but seem to be several times weaker than for the ^{40}Ca(3$^-$) level.

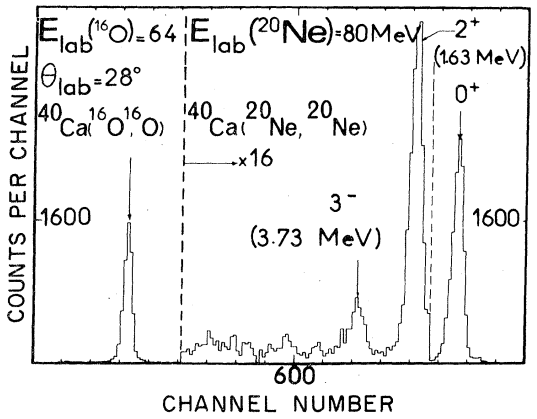

FIG. 1. Scattering of ^{20}Ne by ^{40}Ca: energy spectrum. The peak at the left is due to a small contamination in oxygen of the incident beam.

The experimental results for the elastic and the inelastic scattering are plotted in Figs. 2–4 together with theoretical calculations discussed below. The error bars take into account the statistical, background, and peak separation uncertainties but do not include the absolute normalization error which is about 2–5% for the elastic scattering and 5–10% for the inelastic scattering. The elastic scattering cross section divided by its Rutherford value present conventional Fresnel diffraction form, whereas Coulomb-nuclear interference effects could be clearly observed on the inelastic angular distributions as well as on the excitation functions of $d\sigma_{inel}/d\sigma_{el}$. Plotted vs the Rutherford closest approach distance

$$D(\theta)=\frac{Z_1 Z_2 e^2}{2E_{c.m.}}(1+\csc\tfrac{1}{2}\theta)$$

the elastic scattering data would cover a range of $D(\theta)$ from 8 to 22 fm and the inelastic results from 8 to 16 fm. The maximum bump of the elastic σ/σ_R ratio and the inelastic interference minimum occurred at about $D(\theta)=12$ fm. In terms of the Frahn's closed formalism,[5] the Coulomb-nuclear

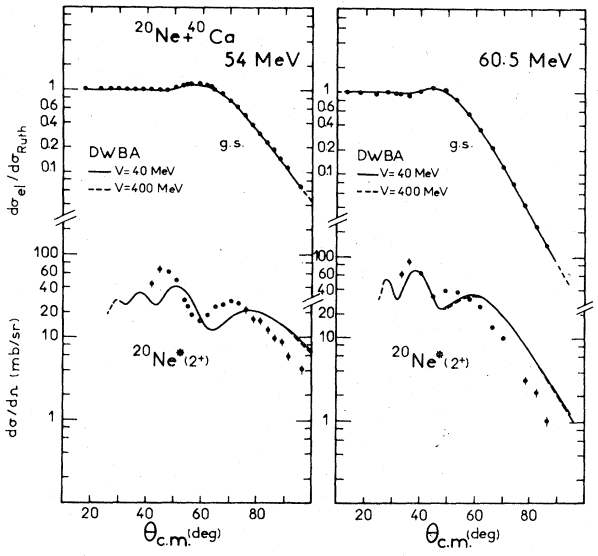

FIG. 2. Angular distributions for the elastic and inelastic scattering. The curves are DWBA calculations using the parameter sets 1 and 4 (solid line); 2 and 5 (dashed line) of Table I.

interference studied in the present work occurred in "the Fresnel diffraction regime where the 180° phase rule represents a purely wave mechanical phenomenon, describing the reversal of the

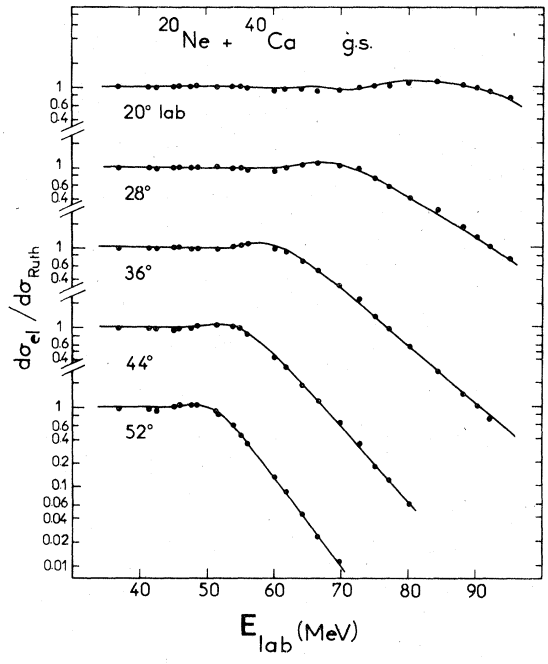

FIG. 3. Excitation functions of the ratio of elastic to Rutherford cross section. The curves are optical model calculations using the parameter set 7 of Table I.

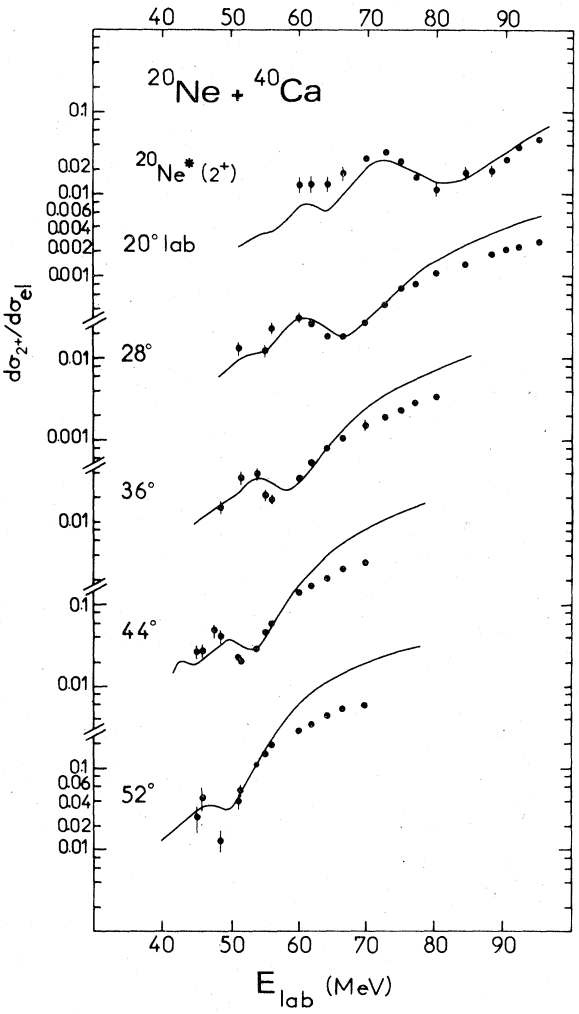

FIG. 4. Ratio of the inelastic cross section to the elastic cross section. The curves are DWBA calculations using the parameter 7 of Table I.

quantal Fresnel oscillation pattern due to the absorptive part of the nuclear interaction."

III. THEORETICAL ANALYSIS

A. Elastic scattering

The angular distributions of the elastic scattering at 54 and 60.5 MeV were analyzed in terms of the optical model by means of the SPI code[16] using a four-parameter potential

$$U(r)=\frac{V_{\mathrm{Coul}}-(V+iW)}{1+\exp[r-r_0(A_1^{1/3}+A_2^{1/3})/a]},$$

where V_{Coul} is the Coulomb potential of an uniformly charged sphere of the same radius as the complex nuclear part. In fact the determination of the real potential strength V is subject to ambiguities,[17,18] particularly when the bombarding ener-

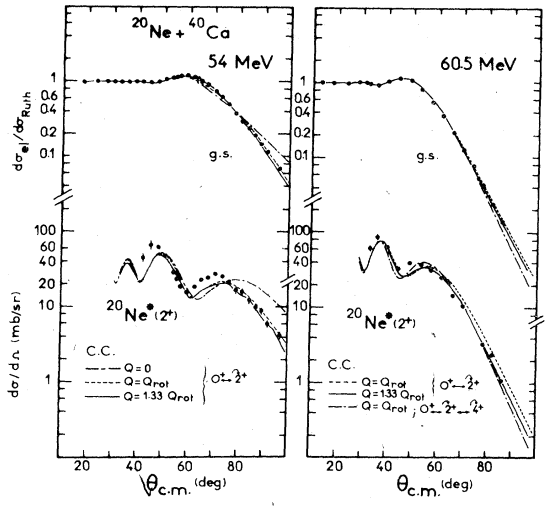

FIG. 5. Angular distribution for the elastic and inelastic scattering. The curves are coupled-channel calculations using the parameter sets 3 and 6 of Table I together with different static quadrupole moment values. A calculation for the 0^{+}-2^{+}-4^{+} coupling with the parameter set 6 is shown in dashed-and-dotted line for 60.5 MeV.

gies are not far above the Coulomb barrier, so that V could be fixed arbitrarily. A gridding search was then done for the imaginary depth W. For each value of W taken in the range $0 < W < V$, the geometrical parameters r_0 and a were adjusted by fitting the angular distributions. The best-fit parameter sets 1 and 4 obtained with $V = 40$ MeV are reported in Table I and the corresponding calculations are shown in Fig. 2.

With the same search procedure, equivalent good fits could be obtained for practically any reasonable value of V. The best-fit W/V ratio is then nearly constant, whereas the radius decreases and the diffuseness increases when V increases.

Plotted as functions of the distance r, the optimum potentials obtained for each angular distribution with different fixed values of V intercept near the closest approach distance of the Rutherford orbit corresponding to the scattering angle $\theta_{1/4}$ where the elastic scattering cross section is equal to a quarter of its Rutherford value. For example, the Fig. 2 shows that the best fits obtained with $V = 400$ MeV are equivalent to those with $V = 40$ MeV. More detailed discussions of these features have been given in previous works.[18-21] The fits were not substantially improved in searches performed with a six-parameter potential using independent form factors for the real and imaginary parts. A four-parameter potential, set 7, could also explain satisfactorily as shown in Fig. 3 the elastic scattering excitation curves, although no energy dependence was taken into account for the parameters.

B. Inelastic scattering

1. Distorted-wave Born approximation

The optical model parameters obtained from the elastic scattering analysis were used in the DWBA calculations for the inelastic scattering with excitation of the first 2^{+} state of ^{20}Ne. The calculations were performed by means of the DWIS code[8] which is a modified version of the DWUCK code.[22] The numerical integration of the transition amplitude was made out to 60 fm for 300 partial waves with the form factor

$$F(r) = F_L^C(r) - \beta^N R_1 \frac{dU(r)}{dr},$$

where the nuclear part is chosen to be proportional to the derivative of the elastic complex optical potential and the Coulomb part is obtained from the electromagnetic transition probability $B(E2)$ by

TABLE I. Optical potential parameters.

Set	E (MeV)	V (MeV)	W (MeV)	r_0 (fm)	a (fm)	$\beta_2^N R$ [a] (fm)	Theory
1	54	40	19	1.27	0.59	2.03	DWBA
2		400	190	1.03	0.61	2.03	DWBA
3		40	3.5	1.27	0.60	1.83	CC
4	60.5	40	24	1.30	0.59	2.03	DWBA
5		400	240	1.03	0.63	2.03	DWBA
6		40	12	1.30	0.58	1.83 [b]	CC
7	36–95	40	25.5	1.25	0.58	2.03	DWBA
8		40	10	1.25	0.57	1.83	CC

[a] $R = r_0 A_1^{1/3}$.

[b] For the 0^{+}-2^{+}-4^{+} coupled-channel calculation in Fig. 5: $\beta_2^N R = 1.52$ fm, $\beta_4^N R = 0.59$ fm, $\beta_2^{Coul} R^2 = 7.83$ fm^2, and $\beta_4^{Coul} R^4 = 17.8$ fm^4.

$$F_L^C(r)=\frac{4\pi Z_2 e[B(EL)]^{1/2}}{2L+1}\begin{cases}\dfrac{1}{r^{L+1}}, & \text{for } r\geq R_{\text{Coul}}\\ \dfrac{r^L}{R_{\text{Coul}}^{2L+1}}, & \text{for } r<R\end{cases}$$

with $R_{\text{Coul}}=r_0A_1^{1/3}$, namely $A_1=Z_2=20$.

In fact the nuclear part is predominantly localized at the nuclear surface, so that it could be neglected for the higher partial waves having impact parameters much larger than the nuclear size. In the present work, the nuclear part was taken into account at least for the first $D_{1/4}/\lambda\!\!\!^{-}+20$ partial waves, $D_{1/4}$ being the Rutherford closest approach distance corresponding to the angle $\theta_{1/4}$ at which the elastic cross section falls off to the quarter of its Rutherford value and $\lambda\!\!\!^{-}$ being the wave length associated to the elastic channel. Typically 75 partial waves were sufficient for both 54 and 60.5 MeV. When the nuclear form factor is neglected, the transition amplitude is calculated with the Samuel-Smilansky method[23] which is faster in computing than the conventional integration.[22]

The deformation length $\beta^N R_1$ in the nuclear form factor was varied to optimize the agreement between the data and the DWBA calculations. The theoretical results shown in Figs. 2 and 4 were obtained with the parameter sets of Table I together with $B(E2)=0.035\ e^2b^2$ value given by Christy and Häuser.[13] The oscillation pattern of the angular distributions is well reproduced; however, the calculations have to be substantially shifted forward to fit the experimental data. Very similar results were obtained with other optical model parameter sets which fitted the elastic scattering data. For example, nearly identical results (Fig. 2) were obtained at 54 MeV for the parameter sets 1 and 2 and at 60.5 MeV for 4 and 5, showing that the inelastic scattering is mostly sensitive to the nuclear surface properties.

With the same nuclear deformation length and $B(E2)$ values, DWBA calculations were performed for the inelastic excitation functions using the parameter set 7. The discrepancies between the theoretical results and the experimental data are similar to those obtained for the angular distributions if the cross sections are plotted in terms of the closest approach distance: The theoretical results are to be shifted out to greater closest approach distances. Such a shift could be performed by an *ad hoc* variation of the nuclear form factor phase[6]; however, the physical meaning of this procedure is not yet quite clear. Coupled-channel calculations should be more appropriate for investigating the second-order effects neglected in the DWBA calculations.

2. Coupled-channel calculations

The coupled-channel (CC) calculations were performed with the *ECIS* code[24] in the framework of the collective rotational model. Because of the strong coupling between the elastic and inelastic channels, the optical model parameters used above for the DWBA calculations have to be modified so as to fit simultaneously the elastic and inelastic data. In fact, acceptable fits could be obtained by lowering the imaginary potential strength and the deformation length together with a small change of the diffuseness parameter.

The CC calculations for the angular distributions obtained with the parameter sets 3 and 6 are compared with the experimental data in Fig. 5. The calculations took into account the 0^+-2^+ coupling with a nuclear deformation length about 10% lower than the DWBA value and with a Coulomb deformation parameter β^{Coul} deduced from the reduced transition probability

$$B(EL)=\left(\frac{3}{4\pi}ZeR_{\text{Coul}}^L\beta^{\text{Coul}}\right)^2$$

with $L=2$ and $B(E2)$ taken from Ref. 13. The nuclear deformation length obtained is in fair agreement with the result furnished by the Hendrie procedure[25] from the Coulomb excitation quadrupole and hexadecapole deformation parameters.[26]

The sensitivity to the reorientation effects were investigated in calculations using different values for the static quadrupole moment Q of the 2^+ state. This sensitivity is strong for small Q values but decreases quickly as Q increases. In Fig. 5 are compared to the experimental data the theoretical angular distributions obtained with $Q=0$, $Q=Q_{\text{rot}}$, and $Q=Q_{\text{exp}}$, where Q_{rot} is the quadrupole moment given by the rotational model and Q_{exp} is the measured value obtained by Nakai *et al.*[14] from Coulomb reorientation effects,

$$Q_{\text{exp}}=-0.24\pm0.03\ \text{b}=(1.33\pm0.18)Q_{\text{rot}}\,.$$

Without the reorientation effect, $Q=0$, the CC curve is similar to the DWBA one shown above in Fig. 2. The last bump of the inelastic angular distributions, particularly at backward angles, is more sensitive to the reorientation effects than the first bump. In fact, the sensitivity should be attenuated if the optical model parameters were readjusted for each value of the Q moment so as to fit the elastic scattering data. Nevertheless, with the parameter sets 3 and 6 the best results were obtained for the measured Q value. Discrepancies still exist particularly in the vicinity of the characteristic interference minimum. Attempts to compensate these discrepancies by taking higher Q moments deteriorated the agreement at back-

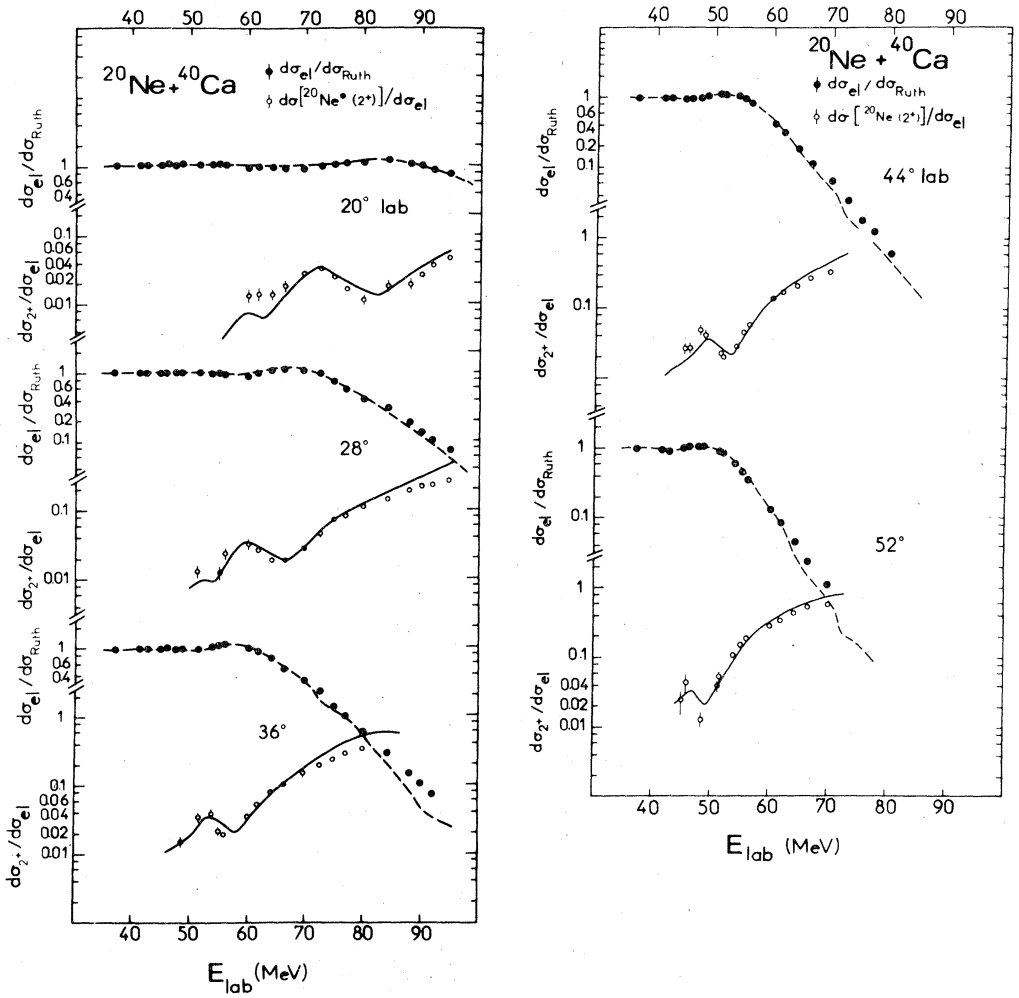

FIG. 6. Excitation functions for the elastic and inelastic scattering. The curves are 0^{+}-2^{+} coupled-channel calculations using the parameter set 8 of Table I.

ward angles.

Effects of the 0^{+}-2^{+}-4^{+} rotational band coupling were also investigated. However, for lack of experimental results for the ^{20}Ne(4^{+}) state, no involved fitting of the data could actually be performed. An example of calculation is shown in Fig. 5 for the 60.5 MeV angular distribution using the parameter set 6. The hexadecapole deformation parameters were taken from Horikawa *et al.*[26] It is not quite clear that the fit could be substantially improved by including the 4^{+} state.

The experimental excitation functions are compared in Fig. 6 to the CC calculations using the 0^{+}-2^{+} coupling together with the parameter set 8 and the measured static quadrupole moment.[14] The inelastic data are better reproduced than by the DWBA calculations particularly at the higher energies which correspond to the smaller closest approach distances.

Attempts to fit the angular distribution data with the procedure suggested by Thorn *et al.*[27] was also made. The differential cross sections of the elastic and inelastic scattering were added and this sum was fitted in a standard optical model calculation with the SPI code.[16] The potential parameters so obtained were used in coupled channel calculations. In fact the fits were not comparable in quality to those obtained above.

IV. CONCLUSION

By measuring two angular distributions and five excitation functions cross sections for the elastic scattering of ^{20}Ne by ^{40}Ca were obtained for Rutherford closest approach distances $D(\theta)$ ranged from 8 to 22 fm. All the angular distributions and the excitation functions of the elastic cross section divided by its Rutherford value present a Fresnel

diffraction form having a maximum bump at about $D = 12$ fm. The data could be reproduced satisfactorily by optical model calculations using a four-parameter complex potential.

Coulomb-nuclear interference effects were experimentally investigated for the inelastic scattering leading to the first 2^+ state of ^{20}Ne. The data were obtained around the elastic maximum bump, covering $D(\theta) = 8$ to 16 fm. Although the DWBA calculations could reproduce the characteristic interference pattern, the theoretical results had to be shifted towards greater closest approach distance, i.e., smaller angle for the angular distributions or smaller energy for the excitation functions, to fit the experimental data. This shift could not be obtained by using different optical model parameters set. Coupled-channel calculations were then used to improve the theoretical analysis by taking into account the strong 0^+-2^+ coupling and the reorientation effects due to the static quadrupole moment Q of the ^{20}Ne(2^+) state. With a Q equal to the measured value[14] the experimental cross sections were substantially better reproduced, particularly at the smaller closest approach distances. However, some discrepancies still exist in the region of the characteristic interference minimum. Although the experimental data were not perfectly reproduced, the inelastic scattering could be useful for checking the static quadrupole moments obtained from other methods.

The authors would like to thank Dr. F. Videbaek for supplying the *DWIS* code and Dr. E. E. Gross for helpful discussions.

[1]S. Landowne, Nukleonika 19, 157 (1974).
[2]K. Alder and A. Winther, in *Electromagnetic Excitation* (North-Holland, Amsterdam/American Elsevier, New York, 1975).
[3]R. A. Broglia, S. Landowne, R. A. Malfliet, V. Rostokin, and A. Winther, Phys. Rep. 11C, 1 (1974), and references therein.
[4]R. A. Broglia, in *Proceedings of the International Conference on Reactions between Complex Nuclei, Nashville, Tennessee, 1974,* edited by R. L. Robinson, F. K. McGovan, J. B. Ball, and J. H. Hamilton (North-Holland, Amsterdam/American Elsevier, New York, 1974), Vol. 2, p. 303.
[5]W. E. Frahn, Nucl. Phys. A272, 2 (1976); and W. E. Frahn and K. E. Rehm, University of Cape Town, South Africa report, 1977 (unpublished).
[6]K. E. Rehm, H. J. Korner, M. Richter, H. P. Rother, J. P. Schiffer, and H. Spieler, Phys. Rev. C 12, 1945 (1975).
[7]P. R. Christensen, I. Chernov, E. E. Gross, R. Stokstad, and F. Videbaek, Nucl. Phys. A207, 433 (1973).
[8]F. Videbaek, P. R. Christensen, O. Hansen, and K. Ulbak, Nucl. Phys. A256, 301 (1976).
[9]M. E. Cobern, N. Lisbona, and M. C. Mermaz, Phys. Rev. C 13, 674 (1976).
[10]D. L. Hillis, E. E. Gross, D. C. Hensley, L. D. Rickersten, C. R. Bingham, A. Scott, and F. T. Baker, Phys. Rev. Lett. 36, 304 (1976).
[11]A. Akiyama, A. Arima, and T. Sebe, Nucl. Phys. A138, 273 (1969).
[12]A. Bohr and B. R. Mottelson, *Nuclear Structure* (Benjamin, Massachusetts, 1975), Vol. 2, p. 96, and references therein.
[13]A. Christy and O. Haüser, Nucl. Data A11, 281 (1972).
[14]K. Nakai, F. S. Stephens, and R. M. Diamond, Nucl. Phys. A150, 114 (1970).
[15]D. Schwalm and B. Povh, Phys. Lett. 29B, 103 (1969).
[16]F. G. Perey, Code SPI (unpublished).
[17]J. S. Blair, in *Proceedings of the Conference on Nuclear Reactions Induced by Heavy Ions, Heidelberg, Germany, 1969,* edited by R. Bock and W. Hering (North-Holland, Amsterdam, 1970).
[18]G. R. Satchler, in Proceedings of the International Conference on Reactions between Complex Nuclei (see Ref. 4), p. 171.
[19]L. West, Jr., K. W. Kemper, and N. R. Fletcher, Phys. Rev. C 11, 859 (1975).
[20]J. Orloff and W. W. Daehnick, Phys. Rev. C 3, 430 (1971).
[21]A. W. Obst, D. L. McShan, and R. H. Davis, Phys. Rev. C 6, 1814 (1972).
[22]P. D. Kunz, code DWUCK, University of Colorado (unpublished).
[23]M. Samuel and U. Smilansky, Phys. Lett. 28B, 318 (1968); Comp. Phys. Comm. 2, 455 (1971).
[24]J. Raynal, Code ECIS, Centre d'Etudes Nucléaires de Saclay (unpublished).
[25]D. L. Hendrie, Phys. Rev. Lett. 7, 473 (1973).
[26]Y. Horikawa, Y. Torizuka, A. Nakada, S. Mitsunobu, Y. Kojima, and M. Kimura, Phys. Lett. 36B, 9 (1971).
[27]C. E. Thorn, M. J. Levine, J. J. Kolata, C. Flaum, P. D. Bond, and J. C. Sens, Phys. Rev. Lett. 8, 384 (1977).